Subharmonic bifurcation cascade of pattern oscillations caused by winding number increasing entrainment

Ch. Jung, B. Huke, and M. Lücke
Institut für Theoretische Physik, Universität des Saarlandes, Postfach 151150, D-66041 Saarbrücken, Germany

Abstract

Convection structures in binary fluid mixtures are investigated for positive Soret coupling in the driving regime where solutal and thermal contributions to the buoyancy forces compete. Bifurcation properties of stable and unstable stationary square, roll, and crossroll (CR) structures and the oscillatory competition between rolls and squares are determined numerically as a function of fluid parameters. A novel type of subharmonic bifurcation cascade (SC) where the oscillation period grows in integer steps as $n\frac{2\pi}{\omega}$ is found and elucidated to be an entrainment process.

PACS: 47.20.Bp, 47.20.Lz, 47.54.+r

Many nonlinear dissipative systems that are driven away from equilibrium by a stationary external forcing respond by spontaneous macroscopic selforganization in time periodic oscillating patterns, e.g., in the form of propagating waves but also in standing structures [1]. A system that, depending on parameters, shows both forms is convection in binary fluid mixtures confined between horizontal plates that impose a vertical temperature gradient: This forcing generates for negative thermodiffusive Soret coupling ψ between temperature and concentration fields propagating convection waves [1]. On the other hand, for $\psi > 0$ periodic pulsations [2–5] of a standing square pattern have been seen such that the intensity oscillations are global and homogeneous along the lines of the squares.

Here we report that and we elucidate how and why such pattern oscillations undergo a SC in which the period τ does not double but increases as $n\frac{2\pi}{\omega}$ with $n = 1, 2, 3, 4, ...$ This peculiar dynamical behavior reflects a novel bifurcation pathway of global pattern oscillations that has not been reported before. To explain it we have to keep track of the bifurcation properties of three different stationary convective structures (squares, rolls, and CRs as explained below). These three states "organize" the dynamical behavior of the system, i.e., of the oscillatory convection. They allow to understand the SC as an entrainment process and to identify the integer n in the SC as the number of windings around a stable CR state of increasing attraction which at the end of the SC becomes sufficiently strong to quench the oscillations.

We have solved the full 3D Oberbeck-Boussinesq hydrodynamic field equations for convection in binary fluids with two different numerical methods: a finite-difference code [6] augmented by a fast multigrid pressure iteration scheme [7] and a Galerkin expansion which also yields unstable 3D solutions. Top and bottom boundaries were rigid, impermeable, perfectly heat conducting plates. Using a 2×2 integration domain in x, y with periodic boundary conditions the wavelength $\lambda = 2$ [8] was fixed to the experimentally observed one [2–4]. A few simulations were done for 16×16 systems with rigid, impermeable, heat insulating side walls to check the robustness of the patterns. We now discuss our findings.

When the thermal stress, i. e., the Rayleigh number is increased the primary stable convective structure for positive Soret coupling, $\psi > 0$, has the form of stationary squares for a wide range of Lewis numbers L and Prandtl numbers σ as predicted by bifurcation theory [9]. Then, convection in the form of pure rolls is an unstable solution. Close to the convective threshold the square structures can roughly be viewed to consist of a superposition of two orthogonal sets of straight parallel stationary convective rolls. We shall call them x-rolls with mode or flow intensity X and wavevector oriented in x-direction and y-rolls, respectively, with mode intensity Y and wavevector in y-direction [10]. In square convection the intensities of the two constitutive rolls are the same, $X_S = Y_S$. For the unstably coexisting pure x-roll solution one has $X_R > 0$ and $Y_R = 0$. The symmetry degenerate pure y-roll solution has $X_R = 0$ and $Y_R > 0$.

We found that the stationary solution branches for squares and rolls are connected by branches of stationary CRs (lines with triangles in Fig. 1) that bifurcate out of the square branch and merge with increasing r with the roll bifurcation branch. Bifurcation properties of these states were unknown so far despite experimental hints for their existence [2,11]. In the CR state the two sets of x-rolls and y-rolls superimpose with different intensities, e. g., $X_{CR} > Y_{CR} > 0$ but equal wave number $k_x = k_y$. These structures differ from the rectangular ($k_x \neq k_y$) CR patterns that grow in pure fluid convection at large r out of

rolls [12]. The transition from CRs to pure rolls is marked by the vanishing of Y_{CR}. In Fig. 1 we identify X_{CR} by upwards (Y_{CR} by downwards) pointing triangles. The CR state with interchanged intensities and dominating y-rolls is symmetry degenerate with the former and corresponds to a convective structure that is rotated by 90°. In addition to the obvious magnitude relations of mode intensities in Fig. 1 like, e.g., $0 \le Y_{CR} \le Y_S = X_S \le X_{CR} \le X_R$ we found for each r shown there that $2X_S \lesssim X_{CR} + Y_{CR} \lesssim X_R$, $N_S \lesssim N_{CR} \lesssim N_R$, and $w_R \le w_{CR} \le w_S \lesssim \sqrt{2} w_R$ [13]. Here the Nusselt number N behaves as $N - 1 \propto (X + Y)$ while the vertical flow amplitude $w \propto (\sqrt{X} + \sqrt{Y})$. In the above relations the CR quantities enter only where they exist, e.g., N_{CR} starts out of the square state with $N_{CR} = N_S$, grows with increasing r, and ends with $N_{CR} = N_R$ in the roll state.

For not too large Lewis numbers, i.e., for *liquid* mixtures the competition between square and pure roll convection leads to the appearance of pulsations of $X(t)$ and $Y(t)$ [2–4]. These oscillations grow in a supercritical Hopf bifurcation out of the square state thereby rendering the latter unstable. Fig. 2 shows for several Rayleigh numbers that $X(t)$ and $Y(t)$ oscillate in opposite phase around a common mean value given by the unstable square state (□ in Fig. 2) such that always $X(t) + Y(t) \cong 2X_S$. The x-roll intensity $X(t)$ of the pulsating pattern grows or decreases on cost of the y-roll intensity $Y(t)$, however, without ever going to zero. Thus the two roll sets never die out completely or reverse their turning direction during the oscillations.

In Fig. 3 we show grey-scale snapshots of the topview shadowgraph intensity distribution $I(x, y)$ taken at times marked in Fig. 2 by A (X minimal; y-rolls dominant), B ($X = Y$; squares), and C (X maximal; x-rolls dominant). After half an oscillating period the pulsating convective structure appears to be rotated by 90° in the $x - y$ plane since $\mathcal{F}(x, y, z; t + \frac{\tau}{2}) = \mathcal{F}(y, -x, z; t)$ holds for the fields $\mathcal{F} = \delta T$ and δC of temperature and concentration, respectively. Furthermore they show always the mirror glide symmetry $\mathcal{F}(x, y, z; t) = -\mathcal{F}(x + \frac{\lambda}{2}, y + \frac{\lambda}{2}, 1 - z; t)$ [14]. The intensity distribution $I(x, y)$ was calculated with the formula [15]

$$I = I^T + I^C \sim r \left(\partial_x^2 + \partial_y^2\right) \int_0^1 dz \, (\delta T + b \, \delta C). \tag{1}$$

The weighting factor b = - 0.43 is for the parameter combination $\psi = 0.23$, $L = 0.0045$, $\sigma = 27$ that can be realized by ethanol-water mixtures [3]. The shadowgraph intensity profile along the dotted line in Fig. 3 B is shown in the bottom right corner together with the contributions I^T and I^C to it from the temperature field and the concentration field, respectively. Narrow concentration plumes caused by the smallness of L generate a narrow central bright stripe in B at the upflow location $x \cong 0.5$ and a peak in I on top of the smooth contribution from δT. This characteristic structure should be easily accessible in experiments.

Close to the Hopf bifurcation the oscillations are harmonic and of small amplitude (Fig. 2a). With increasing thermal driving r the frequency decreases roughly linearly [3] (for example, in Fig. 1 the Hopf frequency is $\omega_H = 0.251$ and $\omega(r = 1.173) = 0.0586$). Furthermore, and more importantly, with increasing amplitude the oscillation becomes more anharmonic and relaxational in Fig. 2b, c; see also Ref. [2,3]: While the system rapidly sweeps through the square state (□) it spends more and more time in the vicinity of the roll state (○). The change from harmonic in Fig. 2a to strongly relaxational oscillations in Fig. 2c is also documented in the right column of Fig. 2. There we show phase space plots X, Y versus $\dot{X}, \dot{Y}$ associated with the time histories of $X(t), Y(t)$ in the left column.

At larger r the system gets attracted into one of the CR fixed points that have become stable shortly below the r-interval marked SC in Fig. 1. In this interval we have observed a novel subharmonic bifurcation cascade in which the CR attractors entrain the oscillations: First the CR attractors deform the phase trajectory (Fig. 2c). Then with increasing r the oscillations execute an increasing number of windings around the CR states (triangles). In Figs. 2c - f the winding number around a CR fixed point increases from $n = 1$ to $n = 4$ and the period τ of the oscillations increases from $\frac{2\pi}{\omega}$ to $n\frac{2\pi}{\omega}$ in integer steps. This increase of the winding number in the SC continues beyond $n = 4$; we have found also $n = 5$. However, the control parameter interval δr_n for an n-cycle becomes so narrow — $\delta r_n \cong (1.6, 0.6, 0.2)10^{-4}$ for $n = (2, 3, 4)$ — that our numerical resources were not sufficient to resolve the SC further. But we think that the SC is a robust, experimentally accessible phenomenon; Ref. [2] contains a hint for a 2-cycle. Beyond the SC interval in Fig. 1 the system gets attracted into one of the CR fixed points. The transition between the oscillations and the CR state is slightly hysteretic. Upon reducing r the system remains in the CR state until below the SC interval and then a transition to an $n = 1$ oscillation occurs. So in a small r- interval there is bistable coexistence of oscillations and stationary CRs.

In Fig. 4 we present phase diagrams in 2D planes of the $r - \psi - L - \sigma$ parameter space. Consider first the $L - r$ plane of Fig. 4a. Upon crossing the bifurcation threshold of the conductive state squares (rolls) become stable at $L \lesssim 0.45$ ($L \gtrsim 0.45$). At smaller ψ we could compare this stability boundary between squares and rolls with results from Ref. [9] and found excellent agreement. The oscillatory regime extends only up to $L \approx 0.02$. This, by the way, explains why oscillations could not be found in the experiments of Ref. [11]. For $L > 0.02$ squares transfer their stability directly to CRs when increasing r.

Consider now the $\psi - r$ plane of Fig. 4b where stable 3D structures are predicted to appear at onset already for $\psi \gtrsim 10^{-7}$ [9]. For the smallest ψ that we have analyzed, $\psi = 0.03$, we found already the full sequence of squares, oscillations, and CRs with increasing r. With growing Soret coupling ψ the stable existence range of each of these 3D structures that are peculiar to mixtures widens on cost of the 2D roll states. The onset of the latter is shifted upward to larger r: With increasing ψ it requires higher thermal stress to generate the flow intensity for which advective mixing is strong enough to eliminate effectively the Soret induced concentration variations that ultimately cause and/or stabilize the 3D structures. Convection in well mixed binary fluids at large r is not much different from one-component fluids. Furthermore, our observation that the ratio of mean squared convective concentration and temperature variations that determine solutal and thermal buoyancy contributions, respectively, is large (small) compared to one at small (large) r sheds light on the oscillatory and/or stationary pattern competition at intermediate r: At small (large) r squares (rolls) are stably sustained by solutally (thermally) dominated buoyancy forces and in the crossover driving regime in between where neither squares nor rolls are stable there is oscillatory and/or stationary pattern competition. As an aside we mention that the advective concentration (heat) transport and the convective concentration (temperature) variation is slightly larger (smaller) in squares than in rolls.

Studying the Prandtl number dependence in Fig. 4c we found that oscillations disappear at $\sigma \lesssim 0.2$ and that rolls appear already slightly above $r = 1$. Increasing σ the existence range of squares, oscillations, and CRs expands to higher r. We have also investigated parameters $L, \sigma = \mathcal{O}(1)$ which apply to *gas* mixtures [16]. Here typically rolls are stable

slightly above onset. Knowledge [17] of their stability domain is useful in relation to the competing spiral defect chaos that has recently been observed also in gas mixtures [16].

Acknowledgments — This work was supported by the Deutsche Forschungsgemeinschaft. The Höchstleistungsrechenzentrum Jülich provided computing time. Numerical support by M. Kamps and M. Fücker is gratefully acknowleged.

REFERENCES

[1] M. C. Cross and P. C. Hohenberg, Rev. Mod. Phys. **65**, 851 (1993).

[2] P. Le Gal, A. Pocheau, and V. Croquette, Phys. Rev. Lett. **54**, 2501 (1985); P. Le Gal, Ph.D. thesis, Université de Paris-Sud, 1986, and private communication.

[3] E. Moses and V. Steinberg, Phys. Rev. Lett. **57**, 2018 (1986); Phys. Rev. A **43**, 707 (1991).

[4] M. A. Dominguez-Lerma, G. Ahlers, and D. S. Cannell, Phys. Rev. A **52**, 6159 (1995).

[5] Theoretical papers investigating these oscillations with different methods and idealizations are, e.g., H. W. Müller and M. Lücke, Phys. Rev. A **38**, 2965 (1988); D. Armbruster, Eur. J. Mech. B Fluids **10**, 7 (1991); M. Bestehorn, Physica D **61**, 59 (1992); Phys. Lett. A **174**, 43 (1993); J. Fernández-Vela and C. Pérez-García, Int. J. Bif. and Chaos **4**, 1333 (1994).

[6] F. H. Harlow and J. E. Welch, Phys. Fluids **8**, 2182 (1965).

[7] Ch. Jung, Ph.D. thesis, Universität Saarbrücken, (1997).

[8] We scale lengths by the thickness d of the fluid layer and times by the vertical heat diffusion time d^2/κ. Thermal diffusivity κ, kinematic viscosity ν, and concentration diffusion coefficient D define Prandtl number $\sigma = \nu/\kappa$ and Lewis number $L = D/\kappa$. Furthermore, we use the reduced Rayleigh number $r = R/R_c^0$ where R_c^0 is the critical one for onset of convection in a pure fluid. The finite-difference calculations were done with homogeneous spatial resolution of 0.05. The Galerkin expansions included wave numbers up to 16π in each direction.

[9] E. Knobloch, Phys. Rev. A **40**, 1549 (1989); T. Clune and E. Knobloch, *ibid* A **44**, 8084 (1992).

[10] In Figs. 1 and 2 we present $X = |I_{10}|^2$ and $Y = |I_{01}|^2$ where I_{nm} are Fourier modes of the topview shadowgraph intensity $I(x, y)$ defined in Eq. (1). Taking instead (Fourier mode) intensities of the velocity fields in x- and y-direction yields practically identical graphs.

[11] P. Bigazzi, S. Ciliberto, and V. Croquette, J. Phys. (France) **51**, 611 (1990).

[12] R. M. Clever and F. H. Busse, J. Fluid Mech. **271**, 103 (1994).

[13] At small r close to threshold we found $X_R \lesssim 2X_S$, $N_R \lesssim N_S$, and $\sqrt{2}w_R \lesssim w_S$ in accordance with a simple amplitude equation that is constructed such as to yield linear growth for $X(r)$ and stable squares [1]. However with increasing r the deviations grow: the intensities of both squares and rolls curve upwards but in different ways such that at $r \gtrsim 0.6$ the above magnitude relations reverse without however rolls becoming stable.

[14] The 2D version of this symmetry was first observed for roll convection at negative ψ: W. Barten, M. Lücke, W. Hort, and M. Kamps, Phys. Rev. Lett. **63**, 376 (1989); W. Barten, M. Lücke, M. Kamps, and R. Schmitz, Phys. Rev. E **51**, 5636 (1995).

[15] S. Rasenat, G. Hartung, B. L. Winkler, and I. Rehberg, Experiments in Fluids **7**, 412 (1989).

[16] J. Liu and G. Ahlers, Phys. Rev. Lett. **77**, 3126 (1996); Phys. Rev. E **55**, 6950 (1997).

[17] B. Huke, P. Büchel, Ch. Jung, and M. Lücke, in preparation; B. Huke, diploma thesis, Universität Saarbrücken, 1997.

FIGURES

FIG. 1. Bifurcation diagram of x-roll intensity X and y-roll intensity Y versus r for squares (squares), rolls (circles), and crossrolls (triangles). Full (dashed) lines with filled (open) symbols denote stable (unstable) states. Full lines delimiting the hatched area mark maxima and minima of oscillations of $X(t)$ and $Y(t)$. A subharmonic bifurcation cascade occurs in the r-interval marked SC (width expanded for better visibility). For the parameters [3] $\psi = 0.23, L = 0.0045, \sigma = 27$ used here stable squares and unstable rolls bifurcate with wave number $k = \pi$ out of the conductive state at $r = 0.0124$ while the critical Rayleigh number is $r_c = \frac{720}{R_c^0}\frac{L}{\psi} = 0.00825$.

FIG. 2. Evolution of the oscillatory dynamics with increasing r from top to bottom. Parameters as in Fig. 1. (a) and (b) are states located shortly above the Hopf threshold and right below the CR bifurcation, respectively. (c) - (f) are SC states. The right column contains phase space plots of X, Y versus $\dot{X}, \dot{Y}$ for $X(t), Y(t)$ shown in the left column with arbitrary common units versus reduced time $n\frac{t}{\tau}$. In the SC states n is the number of windings around each of the stable CR fixed points (triangles). Squares and circles indicate unstable square and roll states, respectively.

FIG. 3. Grey-scale snapshots of topview shadowgraph intensity distribution $I(x, y)$ evaluated with Eq. (1) for the oscillatory state of Fig. 2b at times marked by A (y-rolls dominant), B (squares), and C (x-rolls dominant). To elucidate the contributions from temperature and concentration we show in the bottom right corner the profiles of I^T, I^C, and $I = I^T + I^C$ along the dotted line in B. Maximal up (down) flow is located in B at $x = y \simeq 0.5$ (1.5).

FIG. 4. Phase diagrams of stable convective states. The narrow SC domain is not shown. Parameters are $\psi = 0.23$ (a, c), $L = 0.0045$ (b, c), and $\sigma = 27$ (a,b). Fig. 1 shows for them a bifurcation diagram along the vertical dotted lines in (a, b). The ordinate scale is logarithmic for $r < 1$ to show the bifurcation threshold $r_{stat}(k = \pi; \psi, L)$ of the conductive state (cond) which was determined with a shooting method. Phase boundaries in (a) between crossrolls and rolls from finite difference (full line) and Galerkin (dashed line) calculations are quantitatively unreliable where they disagree at small L combined with large r, i. e., when narrow concentration boundary layers occur in the fluid.

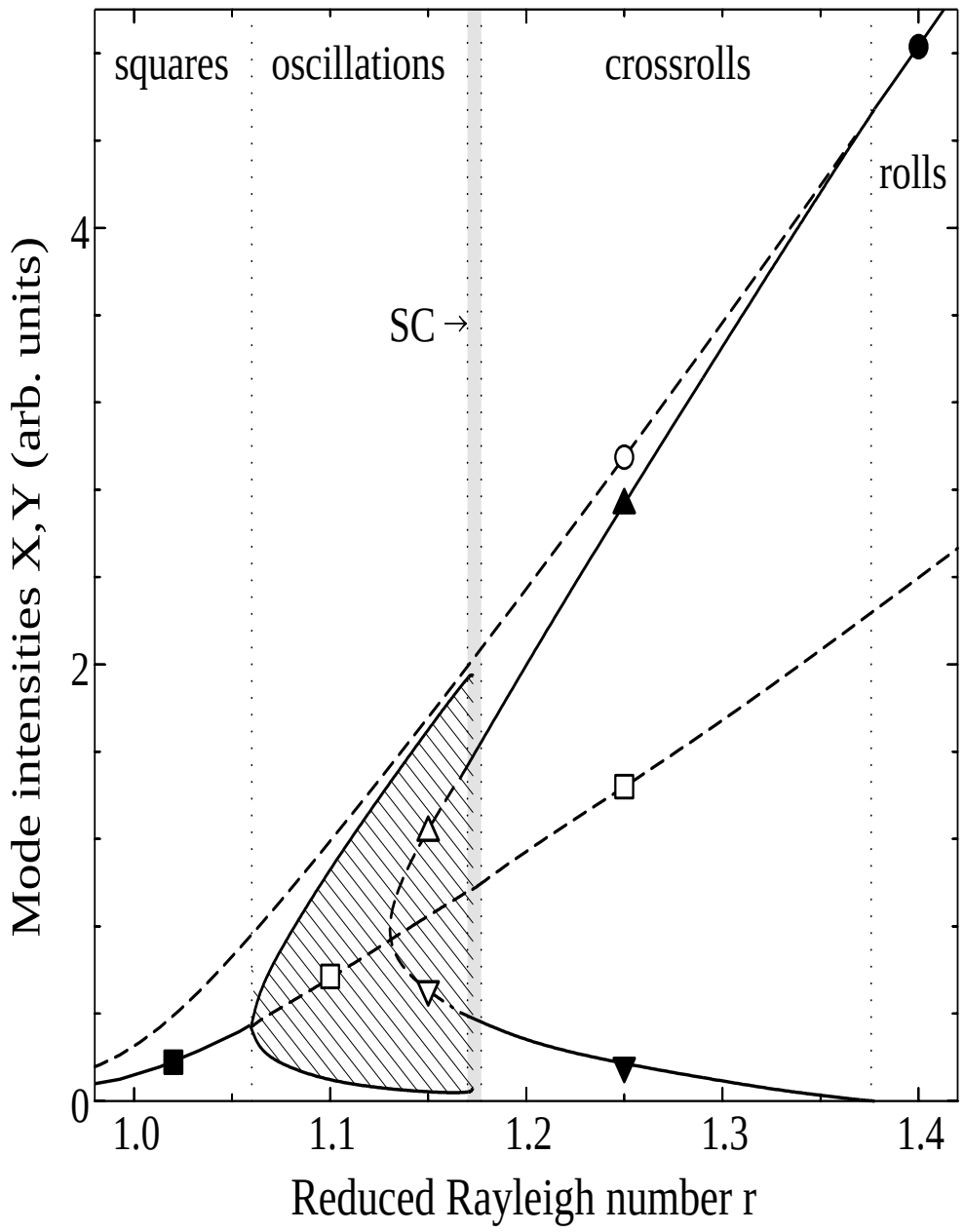

Figure 1

Subharmonic bifurcation cascade of pattern oscillations caused by winding number increasing entrainment

Ch. Jung et al., PRL

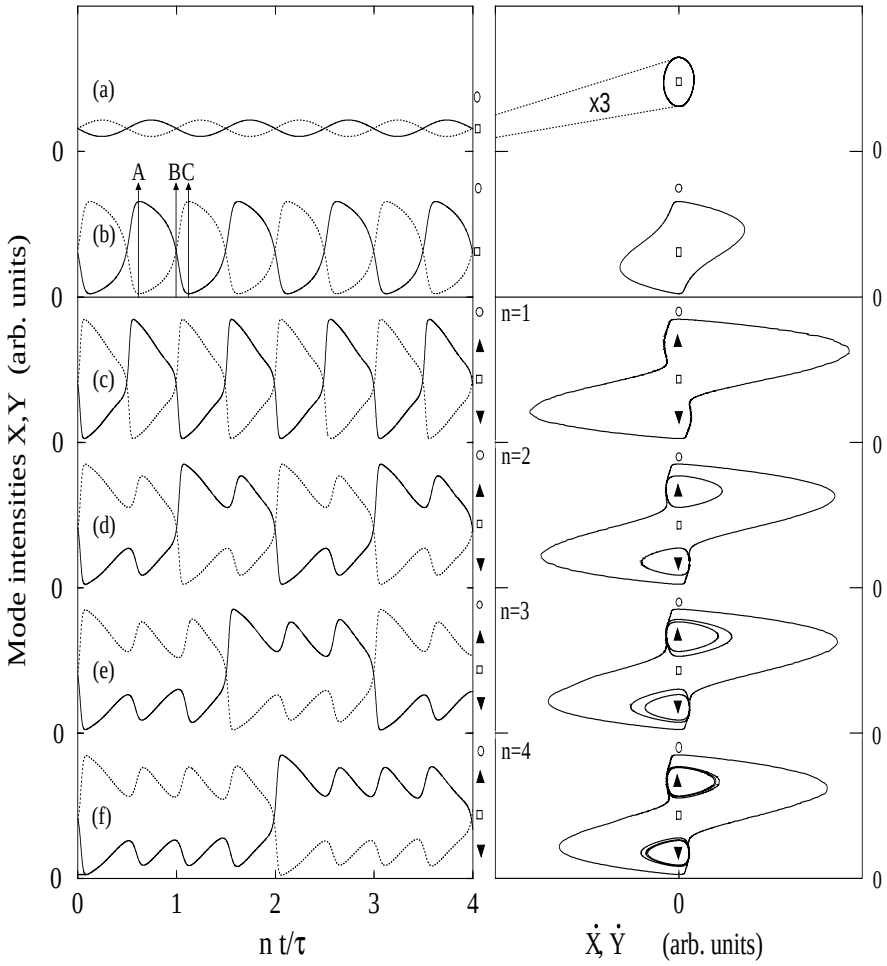

Figure 2

Subharmonic bifurcation cascade of pattern oscillations caused by winding number increasing entrainment

Ch. Jung et al., PRL

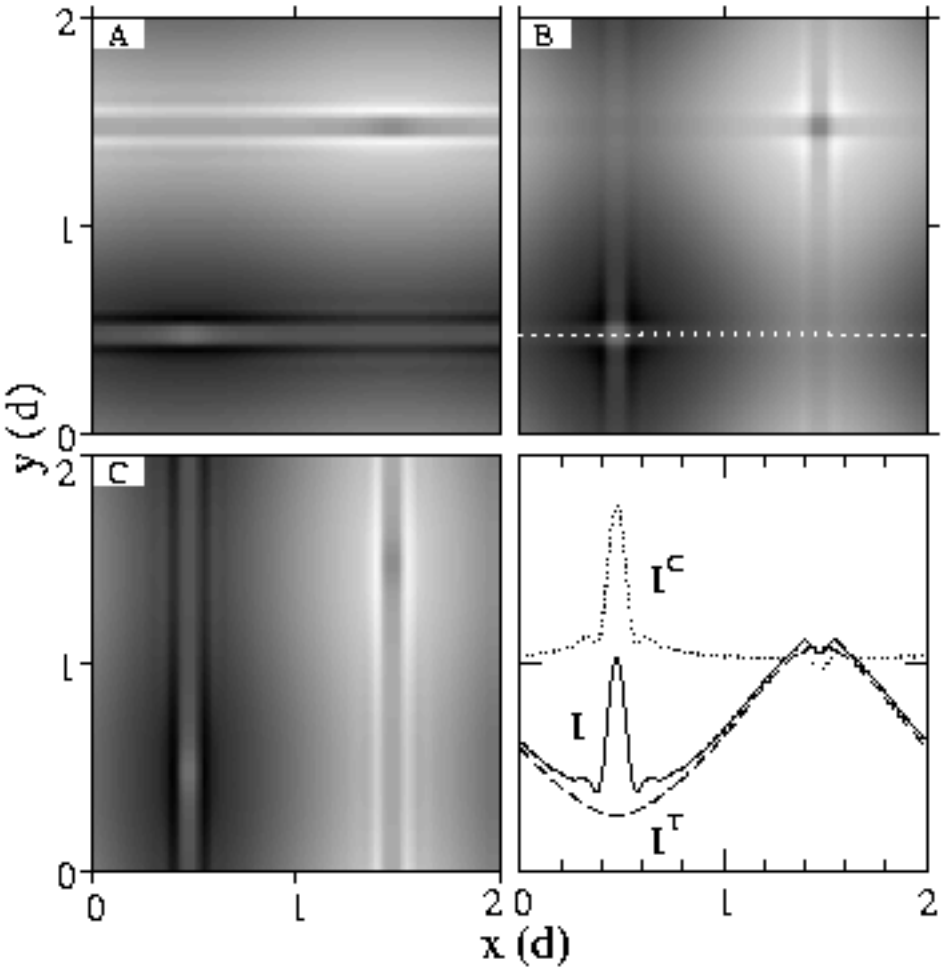

Figure 3

Subharmonic bifurcation cascade of pattern oscillations caused by winding number increasing entrainment

Ch. Jung et al., **PRL**

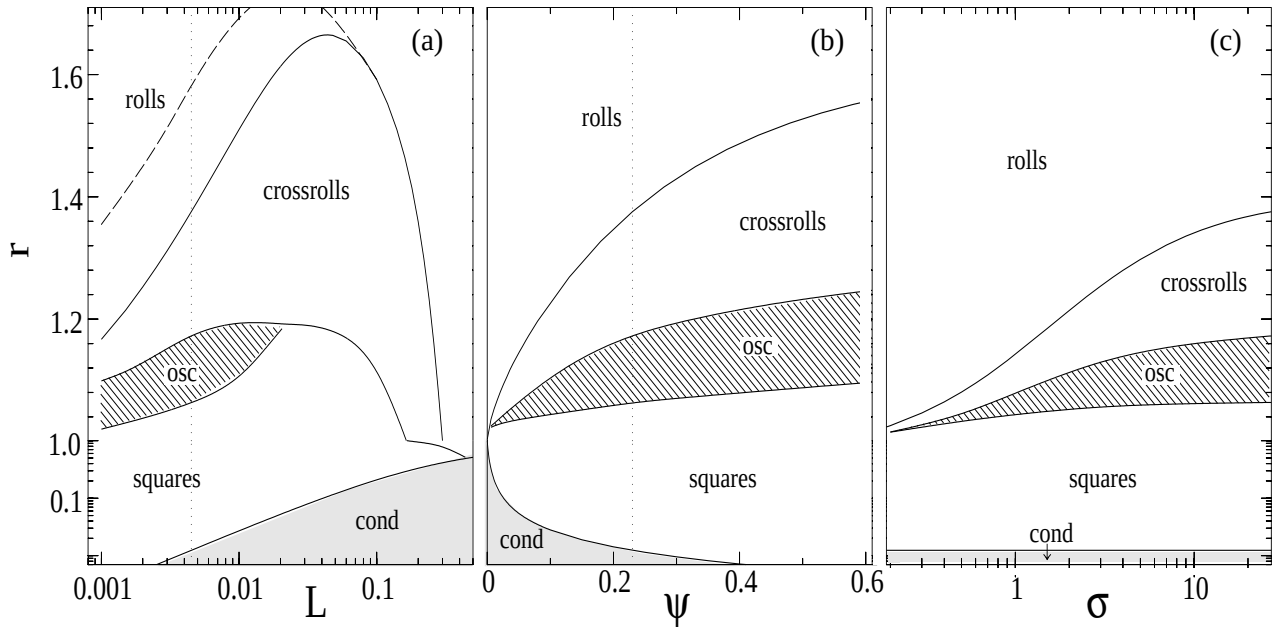

Figure 4

Subharmonic bifurcation cascade of pattern oscillations caused by winding number increasing entrainment

Ch. Jung et al., PRL